



Global distribution of ULF waves during magnetic storms on 27 March and 4 April, 2017: BATSUS+CRCM and Arase observations comparison

Naoko Takahashi⁽¹⁾, Kanako Seki⁽¹⁾, Mariko Teramoto⁽²⁾, Mei-Ching Fok⁽³⁾, Ayako Matsuoka⁽⁴⁾, and Nana Higashio⁽⁵⁾

(1) Graduate school of Science, The University of Tokyo, Tokyo, Japan.

(2) Institute for Space-Earth Environment Research, Nagoya University, Nagoya, Japan.

(3) NASA Goddard Space Flight Center, Greenbelt, Maryland, USA.

(4) Institute of Space and Astronautical Science, Japan Aerospace Exploration Agency, Kanagawa, Japan.

(5) Japan Aerospace Exploration Agency, Tsukuba, Japan.

Abstract

Arase satellite successfully detected ULF waves associated with magnetic storms that occurred from the end of March to April. In this study, we use the Comprehensive Ring Current Model (CRCM) with a global MHD model Block-Adaptive Tree Solar-wind Roe Upwind Scheme (BATSUS) to understand the global distribution of ULF waves during magnetic storms on 27 March 2017 and 4 April 2017. CRCM with BATSUS can reproduce ULF waves with the frequency of 2–3 mHz around post-midnight sector during 27 March storm, which is consistent with the result of Arase satellite. We also compare ULF wave activities between 27 March and 4 April storms. In 27 March storm, the acceleration of relativistic electrons and intermittent activities of ULF waves are seen during the recovery phase, while such activities are not seen in 4 April storm. The existence of ULF wave may contribute the recovery phase duration of magnetic storms.

1. Introduction

The relativistic electron population in the Earth's outer radiation belt is drastically variable, especially during the active condition of the magnetosphere such as magnetic storms. One of the candidate mechanisms to cause the increase or decrease of relativistic electrons is the radial diffusion of electrons driven by ultra-low-frequency (ULF) waves in Pc5 frequency ranges (1.6–6.7 mHz). Therefore, it is important to understand the contribution of ULF waves to the variation of the relativistic electron population during magnetic storms.

There are two drivers of the excitation of ULF waves: external and internal sources. The external source is interpreted as the variability of the solar wind parameters. That is, ULF waves can be excited by the Kelvin-Helmholtz instability at the magnetopause flank [1] and the propagation of compressional waves triggered by the quasi-periodic compression of the solar wind [2]. The dominant mode of solar wind driven-Pc5 is toroidal mode (azimuthal component of magnetic field (B_{ϕ}) and radial component of electric field (E_r)). On the other hand, the

internal source is interpreted as the low-frequency instability of ring current plasma as known as the storm-time Pc5 [4]. The dominant mode is poloidal (B_r and E_{ϕ}). Many previous statistical studies have investigated when, where and how ULF waves excite in the magnetosphere. For example, statistical investigation using ground magnetometer data have clarified the effect of solar wind condition on the occurrence of ULF waves [5]. However, the temporal and spatial distributions during the individual storm are still open to discuss. Especially, it is hard to investigate the longitudinal and radial distribution of ULF waves using only observations, even multiple direct measurements. Therefore, the comprehensive study using a combination of direct measurements and numerical simulations plays an important role to understand the global distribution of ULF waves in the inner magnetosphere. In this study, we aim to understand the global extent of ULF waves during magnetic storms using the global magnetohydrodynamic (MHD) simulation and in situ observation. The first subject of focus is the reproduction of observed ULF waves on 27 March storm using a global MHD simulation coupled with ring current model. The second subject of focus is the comparison of ULF wave activities between different storms.

2. Model description and instrumentation

2.1 Model description

We use the Comprehensive Ring Current Model (CRCM) [6] with a global MHD model Block-Adaptive Tree Solar-wind Roe Upwind Scheme (BATSUS) [7]. Comparing to stand-alone BATSUS simulations, CRCM with BATSUS can solve not only the global magnetospheric dynamics but also the drift physics driven by the plasma pressure motion associated with the ring current. Since this model does not include plasma instabilities, we expect that CRCM with BATSUS can only reproduce ULF waves driven by the quasi-periodic compression of the solar wind. The detailed coupling method between BATSUS and CRCM is described in Glocer et al. [2013] [8].

The simulation box of BATSRUS is from $32 R_E$ (upstream) to $224 R_E$ (downstream), and the size of magnetosphere is $64 R_E$. The inner boundary position is $2.5 R_E$. The coupling region between BATSRUS and CRCM is $8\text{--}10 R_E$. In order to describe the global distribution of ULF waves in the inner magnetosphere, we have request the increased grid resolution in the inner magnetosphere with $0.25 \times 0.25 \times 0.25 R_E^3$. The output of simulation data has a fine time resolution of 10 s. As an input parameter, we use the observed solar wind data obtained from OMNI database. Figure 1 shows the solar wind data and the E-t diagram of relativistic electrons observed by Arase/XEP (as described later) during 26–30 March. Solar wind parameters in Figure 1 indicate that 27 March storm is driven by solar wind dominated by co-rotating interaction region (CIR). Vertical lines in Figure 1 correspond to the timing of each global distribution shown in Figure 2 (as described later).

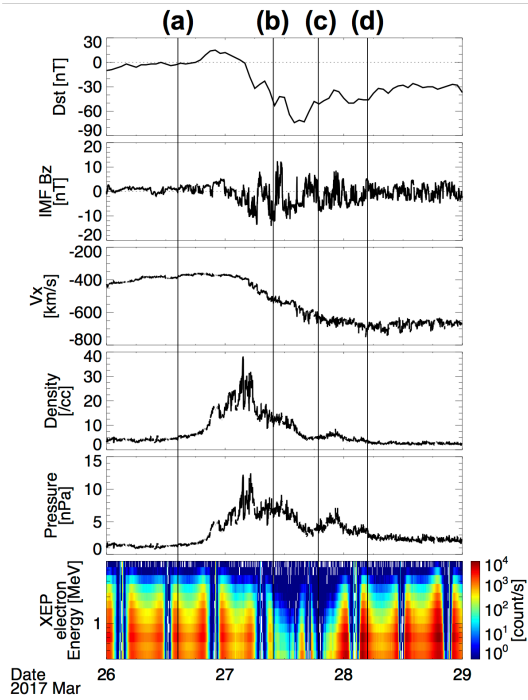


Figure 1. The input parameters to CRCM with BATSRUS. Solar wind data (top five panels) are obtained from OMNI database. The bottom panel shows the E-t diagram of relativistic electron flux derived by Arase/XEP.

2.2 Instrumentation

In order to evaluate the simulation result, we use Arase satellite data that was successfully launched on 20 December 2016. Arase satellite observe electromagnetic fields covering a wide frequency range and charged particles over a wide energy range. In order to identify ULF waves, we use the magnetic field data observed by Magnetic field experiment (MGF) with time resolution of 8 s. We also refer the flux data of relativistic electrons observed by Extremely high-energy electron experiment (XEP) with the energy range of 400 keV–20 MeV in order to identify the condition of radiation belt.

3. Result

3.1 Reproduction of 27 March 2017 storm

First, we reproduce 27 March 2017 storm using CRCM with BATSRUS. Figure 2 shows global distributions of total pressure (color) and flow velocity (vector) calculated from CRCM with BATSRUS at the X-Y plane in Geocentric Solar Magnetospheric (GSM) coordinate.

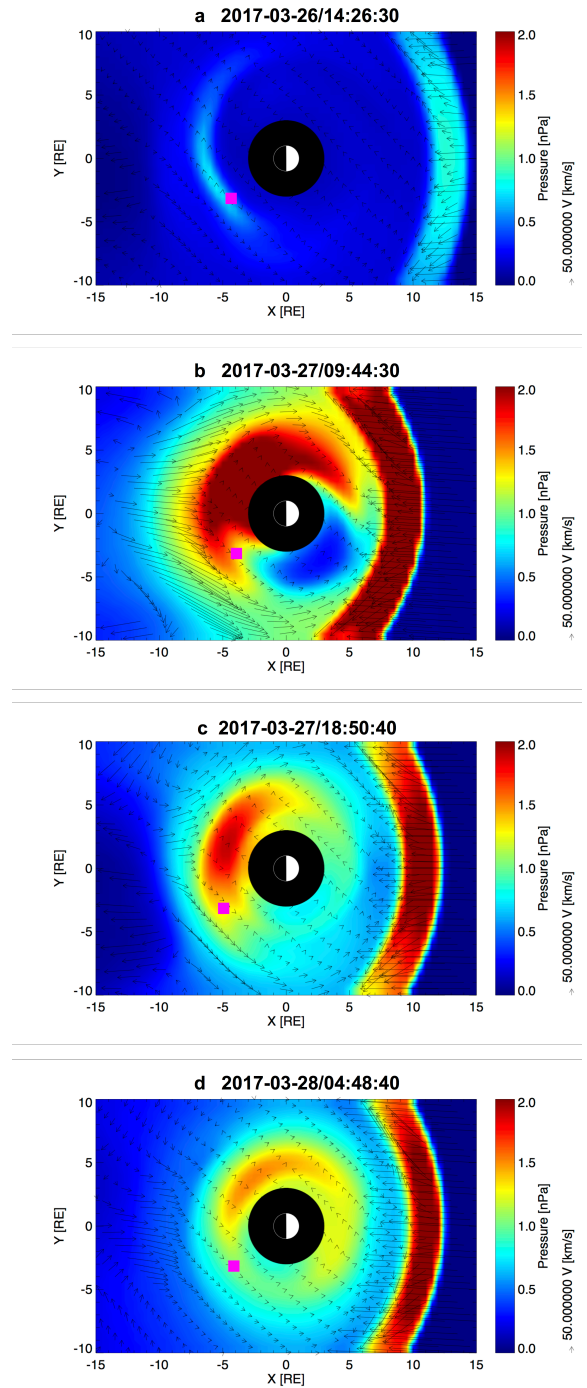


Figure 2. (a)–(f) The distribution of total pressure (color) and flow velocity (arrow) at $Z=0$. The magenta square indicates the Arase satellite position on the equatorial plane.

ULF waves were observed by Arase at 1826–1920 UT on 27 March 2017, as shown in Figure 2c. The magenta square indicates the Arase satellite position on the equatorial plane. Associated with the main phase, the distribution of the total pressure has an asymmetric structure corresponding to the partial ring current (Figure 2b). From around 1730 UT, the total pressure has a quasi-periodical variation globally (cannot show here), which is triggered by the quasi-periodic compression of the solar wind. During the recovery phase, the distribution of the total pressure becomes symmetric (Figure 2f).

3.1.2 Comparison of ULF wave power with Arase satellite data

Figure 3 shows the comparison between the magnetic field data observed by Arase/MGF (Figure 3a–3d) and derived from the simulation result (Figure 3e–3h) during 27 March storm. Figure 3a and 3e show the waveform of the magnetic field, and Figure 3b–3d and Figure 3f–3h show the power spectra of the magnetic field derived by the wavelet analysis. The coordinate is the mean field-aligned coordinate. That is, B_{\parallel} (red) is parallel to the background magnetic field defined as the averaged magnetic field by taking 15 min running averages of in situ magnetic field data, and B_r (blue) and B_{ϕ} (green) are radially outward and eastward components perpendicular to the background magnetic field. As shown in Figure 3f and 3g, the simulation result shows that ULF waves with the frequency of 2–3 mHz are seen in both the poloidal (radial) and toroidal (azimuthal) components, which is consistent with the observational result (Figure 3b and 3c). Comparing the waveform, however, the amplitude of magnetic field derived from the simulation result is a fourth or fifth of the observational result. In addition, the high-frequency wave observed around 1800–1830 UT cannot be reproduced. These results are caused by the rough Cartesian grid of BATSRUS.

3.2 Comparison between 27 March and 4 April storms

Next, we compare the comparison of ULF wave activities between 27 March and 4 April storms that are different in the solar wind structure. Unlike 27 March storm, 4 April storm might be driven by solar wind dominated by coronal mass ejection (CME). Figure 4 shows the comparison of the acceleration of relativistic electrons and Pc5-range wave power (frequency range: 1.6–6.7 mHz) during 27 March (Figure 4a–4c) and 4 April (Figure 4d–4f) storms. The Pc5-range wave power shown at the bottom panel is derived from the integration of simulation data at $L=4.0$ – 7.5 . So far, simulation data are azimuthally integrated because we want to understand the overall response to the variation of Dst index.

During 27 March storm, the flux of relativistic electrons decreases at the main phase and then suddenly accelerates at the recovery phase as shown in Figure 4b. Figure 4c shows that both poloidal (radial, black) and toroidal (azim-

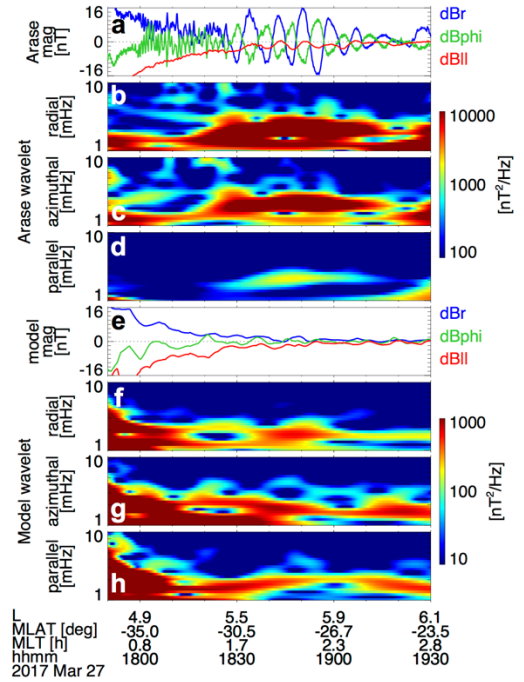


Figure 3. Comparison between Arase (Figure 3a–3d) and simulation (Figure 3e–3h) data. The line plot shows the magnetic field data in the mean field-aligned coordinate (blue: radial, green: azimuthal, and red: parallel to the background magnetic field). The color panels show power spectra of each component of magnetic field.

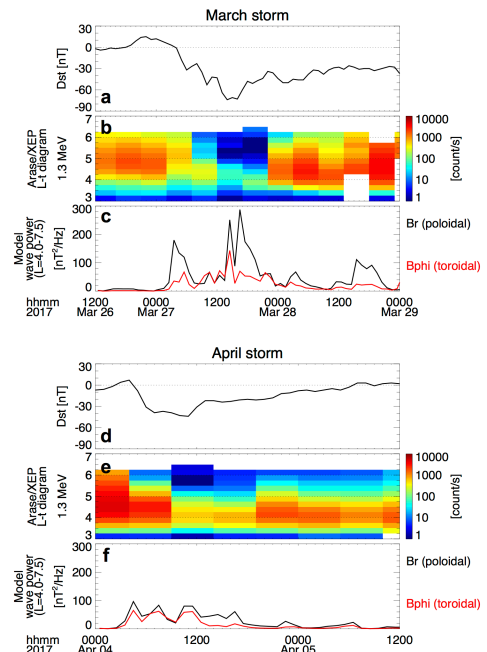


Figure 4. Comparison between relativistic electron flux observed by Arase/XEP and Pc5-range wave power derived by simulation during 27 March (a–c) storm and 4 April storm (d–f). (a, d) Dst index. (b, e) L-t diagram of relativistic electron flux (1.3 MeV) derived from Arase/XEP. (c, f) Pc5-range wave power (1.6–6.7 mHz) estimated from simulation data at $L=4.0$ – 7.5 . The black (red) line indicates the radial (azimuthal) component of magnetic field.

uthal, red) components of Pc5-range wave power are large at the main phase. Note that the intermittent activity of ULF waves is also seen during the recovery phase but its amplitude is smaller than that during the main phase. On the other hand, during 4 April storm, relativistic electrons recover to the pre-storm level rather than accelerate as shown in Figure 4e. Comparing to 27 March storm event, Pc5-range wave power during the main and recovery phases is not so active. Note that the chorus, which is known as another driver of relativistic electron acceleration, are also seen during the recovery phase of 27 March storm. However, during 4 April storm, such chorus activity is not seen.

4. Discussion

As described above, ULF wave activities are seen during the main phase of 27 March storm. It is known that the active wave power at the main phase is mainly triggered by the quasi-periodic variation of solar wind dynamic pressure. Therefore, we can conclude that CRCM with BATSRUS can reproduce ULF waves driven by the quasi-periodic compression of magnetosphere by the solar wind. On the other hand, CRCM with BATSRUS cannot sufficiently reproduce ULF wave activities during the recovery phase of 27 March storm. Because ULF waves during the recovery phase are caused by not only compressional waves due to the magnetospheric compression but also the plasma instabilities such as Kelvin-Helmholtz instabilities, CRCM with BATSRUS cannot reproduce sufficiently.

In addition, comparing to 27 March storm, the acceleration of relativistic electrons during the recovery phase is not seen in 4 April storm event. The possible reason is that both ULF waves and chorus do not occur. As a next step, we have to investigate how much ULF waves contribute the acceleration of relativistic electrons, especially comparing to the chorus. Further event studies will be required in order to estimate the ratio of the contribution of each wave on the acceleration of relativistic electrons.

4. Conclusion

We have reproduced ULF waves using CRCM with BATSRUS during 27 March and 4 April storms. Comparing to the Arase result, CRCM with BATSRUS can quantitatively reproduced ULF waves associated with the quasi-periodic compression of the solar wind during 27 March storm. However, high-frequency waves such as Pc4 or Pi2 pulsations cannot be reproduced due to the rough grid.

We have also compared the flux of relativistic electrons and ULF wave activity. In 27 March storm event, the acceleration of relativistic electrons and related ULF waves are seen during the recovery phase. However, in 4 April storm event, such activities are not seen. Considering that the tendency of chorus activities is the same as that of ULF waves, it is concluded that both ULF waves and chorus play crucial roles of accelerating relativistic electrons. It is notable that further event studies will be required to

estimate the ratio of the contribution of each wave on the acceleration of relativistic electrons.

5. Acknowledgements

Simulation results have been provided by the Community Coordinated Modeling Center at Goddard Space Flight Center through their public Runs on Request system (<http://ccmc.gsfc.nasa.gov>). BATSRUS with CRCM model was developed by Tamas Gombosi (CSEM, Michigan Univ.) and Mei-Ching Fok (NASA, GSFC). Science data of Arase satellite were obtained from the ERG Science Center operated by ISAS/JAXA and ISEE/Nagoya University (<http://ergsc.isee.nagoya-u.ac.jp/>). NT and KS are the members of the PWING (study of dynamical variation of Particles and Waves in the Inner magnetosphere using Ground-based network observations) project supported by Grants-in-Aid for Scientific Research (16H06286) of Japan Society for the Promotion of Science.

6. References

1. Southwood, D. J. (1968), The hydromagnetic stability of the magnetopause boundary, *Planet. Space Sci.*, **16**, 587–605, doi:10.1016/0032-0633(68)90100-1.
2. Kepko, L., H. E. Spence, and H. J. Singer (2002), ULF waves in the solar wind as direct drivers of magnetospheric pulsations, *Geophys. Res. Lett.*, **29**(8), 1197, doi:10.1029/2001GL014405.
3. Takahashi, K., and A. Y. Ukhorskiy (2007), Solar wind control of Pc5 pulsation power at geosynchronous orbit, *J. Geophys. Res.*, **112**, A11205, doi:10.1029/2007JA012483.
4. Southwood, D. J. (1976), A general approach to low-frequency instability in the ring current plasma, *J. Geophys. Res.*, **81**, 3340–3348.
5. Takahashi, K., K. Yumoto, S. G. Claudepierre, E. R. Sanchez, O. A. Troshichev, and A. S. Janzhura (2012), Dependence of the amplitude of Pc5-band magnetic field variations on the solar wind and solar activity, *J. Geophys. Res.*, **117**, A04207, doi:10.1029/2011JA017120.
6. Powell, K. G., P. L. Roe, T. J. Linde, T. I. Gombosi, and D. L. de Zeeuw (1999), A solution-adaptive upwind scheme for ideal magnetohydrodynamics, *J. Comput. Phys.*, **154**, 284–309, doi:10.1006/jcph.1999.6299.
7. Fok, M.-C., R. A. Wolf, R. W. Spiro, and T. E. Moore (2001), Comprehensive computational model of Earth's ring current, *J. Geophys. Res.*, **106**, 8417–8424, doi:10.1029/2000JA000235.
8. Glocer, A., M. Fok, X. Meng, G. Toth, N. Buzulukova, S. Chen, and K. Lin (2013), CRCM + BATS-R-US two-way coupling, *J. Geophys. Res. Space Physics*, **118**, 1635–1650, doi:10.1002/jgra.50221.